Growth of biaxially textured $Ba_xPb_{1-x}TiO_3$ ferroelectric thin films on amorphous Si_3N_4

Rhett T. Brewer,[a] David A. Boyd, Mohamed Y. El-Naggar, Stacey W. Boland, Young-Bae Park, Sossina M. Haile, David G. Goodwin, and Harry A. Atwater
Division of Engineering and Applied Science, California Institute of Technology, Pasadena, California 91125

(Received 8 March 2004; accepted 22 August 2004; published online 30 December 2004)

We prepared highly aligned, biaxially textured $Ba_xPb_{1-x}TiO_3$ (PBT) on amorphous Si_3N_4 by using an ion-beam-assisted deposited MgO as a template layer. PBT was deposited on a biaxially textured MgO using sol-gel synthesis, metal-organic chemical-vapor deposition, and molecular beam epitaxy. The biaxial texture of the PBT was inherited from the MgO template. The reflection high-energy electron diffraction (RHEED) and cross-section transmission electron microscopy (TEM) experiments suggest that exposure of the MgO template to atmospheric moisture before PBT heteroepitaxy resulted in a significant narrowing of the PBT in-plane orientation distribution. The microstructures of the biaxially textured PBT films were analyzed by x-ray diffraction, RHEED, and TEM. The dynamic contact mode electrostatic force microscopy polarization hysteresis loops confirmed that these films are ferroelectric.
 [DOI: 10.1063/1.1806994]

I. INTRODUCTION

The vertical integration of microelectromechanical systems (MEMS) with silicon electronics could be an important pathway for the next generation of device miniaturization, as well as for increased device functionality. A greater latitude in silicon electronics integrated MEMS active materials choice could be achieved by fabricating MEMS devices during a backend process, i.e., after the silicon electronics have been fabricated and protected from contamination. One of the challenges with this approach is that the surfaces available for growth (metal layers and low-k dielectric materials) are not single crystalline and not suitable for heteroepitaxy. A flexible materials integration strategy that allows for the growth of new materials on amorphous surfaces is desirable. One class of materials that possesses interesting properties for MEMS applications, which is incompatible with conventional silicon electronics processing but could potentially be integrated with silicon following this strategy, are perovskite ferroelectrics.

High-strain ferroelectrics, such as $BaTiO_3$ and $PbTiO_3$, are candidates for actuator materials because they combine high work/volume with high-frequency response. One possible route for ferroelectric/silicon integration is to create biaxially textured ferroelectrics using a buffer layer as a heteroepitaxial template. The biaxially textured materials are polycrystalline with preferred in-plane and out-of-plane crystallographic orientations, where the degree of alignment is characterized by the full width at half maximum (FWHM) of the orientation distribution around the nominal zone axis direction. Using ion-beam-assisted deposition (IBAD), the biaxially textured films can be fabricated on amorphous surfaces. Wang *et al.* demonstrated that the IBAD MgO on amorphous Si_3N_4 develops a narrow biaxial texture in the films only 11-nm thick.[1] Previous work has demonstrated the heteroepitaxy of $BaTiO_3$ and $PbTiO_3$ on a (001) single-crystal MgO. The out-of-plane orientation was defined by $[001]_{Ferro}$ parallel to $[001]_{MgO}$ and the in-plane orientation by $[100]_{Ferro}$ parallel to $[100]_{MgO}$.[2,3] It is therefore expected that heteroepitaxial perovskite ferroelectrics will reproduce the biaxial texture of the MgO template.

The literature is silent on the properties of biaxially textured, perovskite ferroelectric thin films. The grain-boundary properties are important for ferroelectric thin-film domain switching, where the trapped charges at the domain walls have been implicated in the domain-wall pinning in lead zirconate titanate.[4] Investigations in superconducting $YBa_2C_3O_{7-x}$ show that the biaxially textured films can exhibit functionality that approaches that of single crystalline material because of the special properties of the low-angle grain boundaries.[5] With the low-angle grain boundaries, it is reasonable to expect that the domain-wall pinning would be reduced in the biaxially textured ferroelectrics. A biaxial texture is also important for polycrystalline actuator performance because the film elongation is directed and switchable only along the (100) crystal planes. A randomly oriented polycrystalline film performs less than half of the actuation that a single-crystal film produces, whereas the biaxially textured ferroelectric films, with a biaxial texture comparable with the IBAD MgO films,[1] can produce over 90% of the single-crystal actuation.

To enable the investigation of the ferroelectric properties of biaxial-textured perovskites, we have grown biaxially textured $Ba_xPb_{1-x}TiO_3$ (PBT) on biaxially textured MgO. $Ba_xPb_{1-x}TiO_3$ is a perovskite ferroelectric, where Ba and Pb equivalently exchange positions on the *A* site of the ABO_3

[a]Author to whom correspondence should be addressed; electronic mail: rhett.t.brewer@intel.com

structure, and the *a*-axis/*c*-axis ratio (the material actuation) can be continuously tuned from 1.01 to 1.06 by changing the fraction of Ba from 1 to 0.[6]

II. EXPERIMENT

A. Film growth methods: Sol-gel synthesis, metal-organic chemical-vapor deposition (MOCVD), and molecular beam epitaxy (MBE)

The biaxially textured MgO films were grown on amorphous Si_3N_4/Si substrates using IBAD. MgO was supplied from an e-beam evaporator at 0.2 nm/s with a simultaneous 1200-eV Ar^+-ion bombardment at a 45° incidence angle. The MgO biaxial texture was controlled by varying the ion/MgO molecule flux ratio during the deposition.[7] The IBAD MgO film was either directly used as a heteroepitaxial template for PBT or was first coated with a 20-nm layer of homoepitaxial MgO grown at 600 °C.

The PBT was grown on biaxially textured MgO using a sol-gel solution system of Pb-acetate trihydrate: Ba-acetate: Ti-isopropoxide dissolved in ethylene glycol in a 1:1:2 ratio, with acetylacetone for Ti chelation in a 4:1 molar ratio.[8] Water was added to the solution such that the molar ratio of H_2O to Ti was eight. This solution was spin coated onto the biaxially textured MgO templates at 4000 rpm, pyrolyzed at 450 °C for 3 min, and then calcined at 600 °C for 2 h. Rutherford backscattering spectroscopy (RBS) measurements show that a single coating following this procedure results in a 47-nm-thick film with a $Ba_{0.55}Pb_{0.45}TiO_3$ composition. This same deposition process was followed for deposition on a (001) single crystalline MgO substrate as well. On the single-crystal film, instead of only one layer, three layers were grown. Each additional layer was deposited after sintering the previous layer at 600 °C.

PBT was also grown using MOCVD in a vertical, stagnation flow reactor. The Ba, Pb, and Ti precursors are $Ba(tmhd)_2$, Pb $(tmhd)_2$, and $Ti(OPri)_2(tmhd)_2$, where tmhds is 2,2,6,6-tetramethylheptane-3,5-dionate and OPri is diisopropoxy. Using Ar as a carrier gas, the precursors are combined in a gas line at 250 °C before being introduced into a mixing chamber with oxygen. The well-mixed gas is introduced into the deposition chamber through a shower head nozzle, where it is deposited onto the MgO substrate at 15 torr and 750 °C.

The stoichiometry is controlled using UV absorption and control loop feedback techniques.[9] The Typical PBT deposition rates are 4 nm/min and the films were grown to about 100-nm thick. PBT was grown on both the biaxially textured MgO substrates and (001) single-crystalline MgO. $Ba_{0.03}Pb_{0.97}TiO_3$ and $Ba_{0.2}Pb_{0.8}TiO_3$ were grown using this method.

MBE was performed at 700 °C by a co-evaporation of 0.40 nm/min Pb (99.999% pure), 1.08 nm/min Ba (99% pure) from effusion cells, and 0.54 nm/min Ti from a Varian Ti-ball sublimation pump[10] with a HP 6673A power supply, as measured with a quartz-crystal monitor prior to the introduction of oxygen into the MBE chamber. The oxygen source was an Oxford Applied Research HD25 rf atom source operating at 500 W with O_2 introduced into the back of the source through a leak valve creating an O_2 partial pressure of 6×10^{-5} torr. The rf atom source has been estimated to have an O_2 cracking efficiency of 30% at 500 W.[11] The film composition, measured using the RBS, was $Ba_{0.67}Sr_{0.03}Pb_{0.002}Ti_{1.3}O_3$ and it was 70-nm thick. The low Pb content can be attributed to an insufficient partial pressure of atomic oxygen for an efficient Pb oxidation.[12] The Sr originated as a 0.5% impurity in the 99% pure Ba source material. The low Ba content resulted from the suppression of Ba evaporation when oxygen was introduced into the MBE chamber.[12]

Despite the unusual film composition, x-ray scattering, transmission electron microscopy (TEM), and reflection high-energy electron diffraction (RHEED) consistently indicate that the crystal structure of the MBE grown film is an ABO_3 perovskite. To be a perovskite film, part of the titanium must substitute for Ba^{2+} in the ABO_3 structure as Ti^{2+}. It is therefore useful to compare the biaxial texture and the film structure of the MBE perovskite film to the films grown using sol gel and MOCVD. Given the absence of Pb in this film, we refer to it hereafter as BT instead of PBT.

B. Film characterization

The ferroelectric film phase purity and *c*/*a*-axis ratios were investigated with x-ray diffraction (XRD). The biaxial texture of the IBAD MgO templates and of the heteroepitaxial ferroelectric films were measured using a RHEED-based technique.[13,8] The quality of the ferroelectric/MgO interface and the film structure were examined with TEM. The ferroelectric behavior of these films was probed using dynamic contact mode electrostatic force microscopy (DC-EFM).[14]

III. RESULTS AND DISCUSSION

Both $BaTiO_3$ and $PbTiO_3$ grow heteroepitaxially on (001) single-crystal MgO with an alignment of the ferroelectric and MgO in-plane and out-of-plane (001) directions,[2,3] so the same heteroepitaxial relationship was expected from PBT on MgO. The crystallographic orientation of PBT and BT deposited on a template layer of the biaxially textured MgO and PBT deposited on (001) single-crystal MgO was measured using x-ray (Cu K_α) diffraction $\theta-2\theta$ curves (Fig. 1). All the films show a (100) and/or (001) orientation [the extra peak at $2\theta=32°$ for the sol-gel sample is Si(002), attributable to the Si_3N_4/Si(001) substrate]. The Pb-rich MOCVD films, with a large difference in the magnitudes of the *a* axis and *c* axis, show a clear tetragonal splitting. For the sol-gel films, with intermediate composition, the difference between the *a* axis and *c* axis is smaller, but a tetragonal splitting can still be observed. In comparison to deposition on a single-crystal MgO, deposition on the biaxially textured template MgO, regardless of the route utilized, produces highly *a*-axis oriented films. This result can be understood in terms of the stresses imposed on the ferroelectric thin film by the coefficient of the thermal-expansion mismatch between them and the substrate.[15,16] The coefficient of the thermal expansion for silicon is 2.59×10^{-6} K, whereas the coefficient of the thermal expansion for MgO is 14.8×10^{-6} K; for

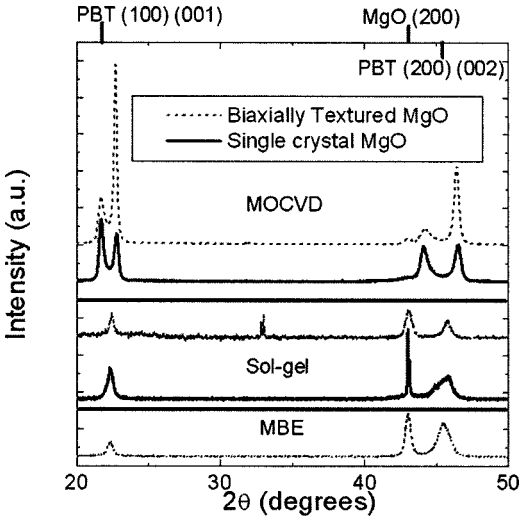

FIG. 1. X-ray $\theta-2\theta$ curves from PBT deposited by MOCVD and sol gel on the single-crystal MgO (001) and biaxially textured MgO. An x-ray $\theta-2\theta$ curve from MBE BT on the biaxially textured MgO is also included.

$PbTiO_3$, it is 12.6×10^{-6} K, and for $BaTiO_3$, it is 9.8×10^{-6} K.[17–19] Because the template layer is extremely thin, the thermal expansion of the substrate for the biaxially textured MgO films is dominated by the silicon wafer. Thus, all the PBT and BT films grown on MgO at a high temperature on the biaxially textured MgO substrates experience tensile stresses upon cool down, resulting in the predominantly *a*-axis oriented films (the longer *c* axis orients parallel to the substrate). In contrast, the films grown on a single-crystal MgO experience a compressive stress during cooling, which promotes the *c*-axis orientation. The *c*-axis component of the MOCVD film grown on a single-crystal MgO is higher than for the sol-gel film, because it was grown at a 150 °C higher temperature and accumulated more compressive stress during cooling.

A. Biaxially textured MgO substrate

The heteroepitaxy of PBT was performed on two types of the biaxially textured MgO templates. The first type of substrate was a 8-nm IBAD $MgO/Si_3N_4/Si(100)$. The second type of substrate was a 20-nm homoepitaxial MgO grown at 600 °C/8-nm IBAD $MgO/Si_3N_4/Si(100)$. The x-ray $\theta-2\theta$ scans of PBT, grown by both sol gel and MOCVD, exhibit much stronger diffraction when grown on the homoepitaxial MgO surfaces (shown in Fig. 1) than when grown on the IBAD MgO surfaces (not shown). While the sol gel on IBAD MgO only displays (h00) diffraction peaks (albeit much weaker than for the films grown on homoepitaxial MgO surfaces), the MOCVD film grown on IBAD MgO displays diffraction peaks from all the possible orientations.

There are also striking differences in the RHEED patterns from the PBT deposited directly on the IBAD MgO surfaces and from the films deposited on the homoepitaxial MgO surfaces. Figure 2 shows the RHEED patterns from the sol gel and MOCVD PBT grown on the IBAD MgO surfaces and on the IBAD MgO films with an additional 20 nm of the homoepitaxial MgO grown at 600 °C. The films grown directly on the IBAD MgO surfaces [Figs. 2(b) and 2(d)] exhibit broad out-of-plane orientation distributions, evident from the broad diffraction rings, which appear instead of the sharp diffraction spots. The out-of-plane orientation distribution cannot be measured for these films using our standard RHEED method because it is only valid for narrow orienta-

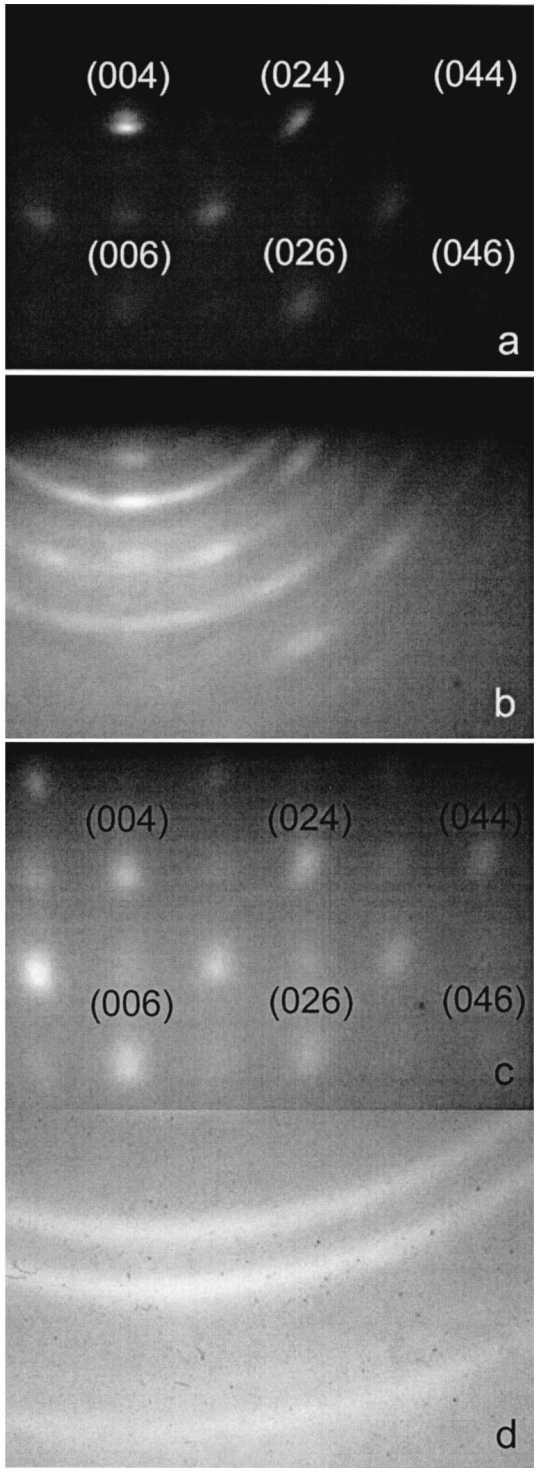

FIG. 2. RHEED images of PBT grown on biaxially textured MgO. Sol-gel (a) and MOCVD (c) PBT RHEED images from the films deposited on the MgO templates made from 8 nm of the IBAD MgO and an additional 20 nm of the homoepitaxial MgO grown at 600 °C. Sol gel (b) and MOCVD (d) PBT RHEED images from the films deposited on the MgO templates made from 8 nm of IBAD MgO.

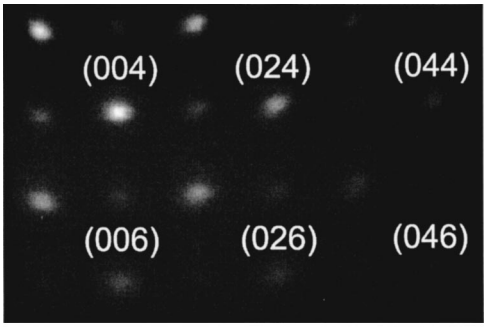

FIG. 3. RHEED image of BT grown heteroepitaxially on biaxially textured MgO made from 8 nm of IBAD MgO and 20 nm of homoepitaxial MgO grown at 600 °C.

tion distributions.[13] The PBT films grown under the same conditions on biaxially textured MgO with a homoepitaxial layer show sharp diffraction spots characteristic of narrow out-of-plane orientation distributions ($\Delta\omega$=3° FWHM for MOCVD and $\Delta\omega$=4° FWHM for sol gel, where $\Delta\omega$ represents the out-of-plane orientation distribution FWHM). All the diffraction patterns in Fig. 2 have significant broad background intensities, which can arise from the scattering from a rough surface, grain boundaries, lattice defects, or amorphous regions in the film.

A RHEED image from a MBE grown BT on a biaxially textured MgO (with a 20-nm homoepitaxial MgO layer) is shown in Fig. 3. The out-of-plane orientation distribution for the MBE film is similar to the out-of-plane orientation distribution measured for the sol gel and MOCVD film ($\Delta\omega$ =2.5° FWHM), however, the diffuse background scattering is much weaker than for the sol-gel and MOCVD films.

The IBAD MgO surfaces may not function as good heteroepitaxial templates for PBT because of the high defect density inherent in ion bombardment processes. Because the heteroepitaxy is generally *ex situ*, the IBAD MgO surface is exposed to moisture from the atmosphere. While water absorbs readily on the MgO(100) surface, experimental evidence and calculations suggest that a perfect MgO(100) surface is stable against hydroxylation, and that MgO dissolution and pitting only occur at the surface defects.[20] The IBAD MgO samples stored in the atmosphere (or even in a nitrogen purge box for extended periods) will change from a smooth mirrorlike surface to a pitted, rough finish. The IBAD MgO samples were exposed to the atmosphere for the minimum possible time before heteroepitaxy, however, some exposure to the atmosphere was inevitable during the sample transfers between the deposition chambers. We speculate that the homoepitaxial layer grown on IBAD MgO reduces the defect density from ion bombardment and makes the substrate less susceptible to damage from water absorption. During one experiment, the homoepitaxial MgO film was left in room ambient overnight before the MOCVD PBT heteroepitaxial growth. The resulting PBT demonstrated biaxial texture commensurate with the MgO template, despite its exposure to the atmospheric moisture. Therefore, the homoepitaxial biaxially textured MgO templates are at least somewhat stable in atmospheric moisture.

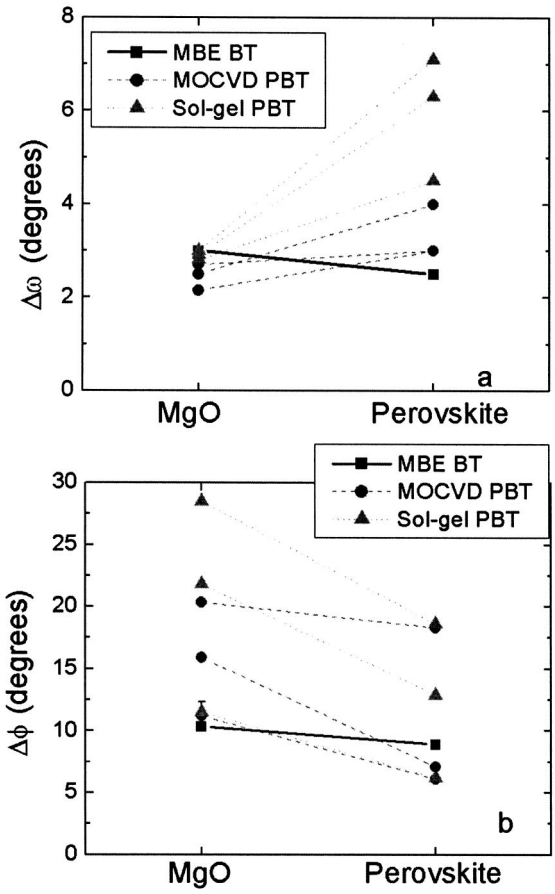

FIG. 4. Out-of-plane ($\Delta\omega$) and in-plane ($\Delta\phi$) orientation distributions of the biaxially textured MgO templates and the heteroepitaxial perovskite (BT or PBT) deposited by MBE, MOCVD, or sol gel.

B. Ferroelectric biaxial texture inheritance

Experiments to study the biaxial texturing of PBT on biaxially textured MgO used the IBAD MgO films with an additional 20 nm of homoepitaxially grown MgO at 600 °C in 3×10^{-5} torr of O_2. The biaxial texture of the MgO template was controlled by changing the ion/MgO flux ratio during IBAD. The homoepitaxial MgO deposition rates varied from 0.15 to 0.03 nm/s (according to the quartz-crystal monitor), but the deposition rate showed no significant effect on the homoepitaxial MgO biaxial texture. We measured the sticking coefficient for MgO at 600 °C to be 0.4, so the actual deposition rates varied between 0.06 nm/s and 0.012 nm/s. A series of biaxially textured MgO templates were grown with various in-plane ($\Delta\phi$) and out-of-plane ($\Delta\omega$) orientation distributions. PBT was deposited on these MgO templates using sol gel and MOCVD. BT was also deposited on biaxially textured MgO using MBE. The biaxial texture of the MgO templates and the heteroepitaxial PBT and BT were measured using RHEED and compared.

A summary of the results from these experiments is shown in Fig. 4, where the out-of-plane ($\Delta\omega$) and in-plane ($\Delta\phi$) orientation distributions are plotted for each sample as a function of the film layer (homoepitaxial MgO and ferroelectric layers). The in-plane orientation distribution measurement for the MBE MgO template is actually from the IBAD MgO surface (the in-plane distribution was not mea-

sured after the homoepitaxial MgO growth and before the BT heteroepitaxy), but based on the previous experiments, the in-plane orientation distribution of the homoepitaxial MgO layer should be within 2° of the in-plane orientation distribution of the IBAD layer. We observe that the ferroelectric inherits, to a large extent, the biaxial texture of the MgO template. The in-plane orientation distribution of the PBT is, in fact, narrower than that of the MgO template. Such behavior has also been observed for heteroepitaxial $YBa_2Cu_3O_{7-x}$ on MgO.[21] The TEM images of MOCVD grown on the biaxially textured MgO show grains, which are 40–80 nm across compared with the 25-nm grains observed in the homoepitaxial MgO. This indicates that the PBT selectively nucleates on the well-aligned grains to create a more highly in-plane aligned film. The out-of-plane orientation of the PBT degrades slightly relative to that of the MgO template, but only by a few degrees. This degradation may result from the roughness of the homoepitaxial MgO template, which is typically measured at 0.8-nm rms by atomic force microscopy (AFM). The MBE grown ferroelectric film exhibited a particularly close correlation between the in-plane orientation distributions of the MgO template and the heteroepitaxial BT. The strong dependence of the PBT and BT biaxial texture on the MgO template biaxial texture confirms that the PBT and BT biaxial texture can be controlled through the MgO template. Therefore, developing processes to optimize the biaxial texture of the MgO template will improve the biaxial texture of the heteroepitaxial ferroelectric materials.

C. Ferroelectric/MgO interface

The MgO/ferroelectric interface and the ferroelectric microstructure were examined using TEM images and diffraction patterns. The quality of the interface was highly dependent on the deposition method.

TEM bright field images of the MOVCD PBT/MgO interface are shown in Fig. 5. Figures 5(a) and 5(b) are examples of two different regions observed for the PBT/MgO interface. In Fig. 5(a) the lattice planes are observable throughout the MgO layer, proving its crystallinity. There is also a clear distinction between the highly damaged IBAD MgO layer (the first 7.8 nm) and the homoepitaxial layer (18-nm thick). However, in Fig. 5(b), the MgO appears to be amorphous, although whether or not it is actually amorphous is uncertain. A high-resolution image of the MOCVD PBT/amorphous-looking MgO template interface clearly shows that the crystal lattice planes of the PBT emerge from the apparently disordered MgO [Fig. 5(c)].

Bright field TEM images show no appreciable difference between the PBT microstructure over the crystalline MgO and the apparently amorphous region. Strong texturing, both in plane and out of plane, of the PBT make it unlikely that the MgO template was (entirely) amorphous before the film growth. MOCVD PBT depositions on amorphous Si_3N_4 result in a weak x-ray diffraction and peaks from all the possible orientations. The deposition on the biaxially textured MgO template only produced diffraction peaks from the (001)/(100) orientation. At least some regions of the MgO layer must have been crystalline to seed this preferred out-of-plane growth direction and then overgrow any amorphous MgO regions present. The plan view TEM images reveal that the biaxially textured PBT average grains size is 60 nm, which means a single PBT grain will overgrow several 20–25-nm MgO grains.

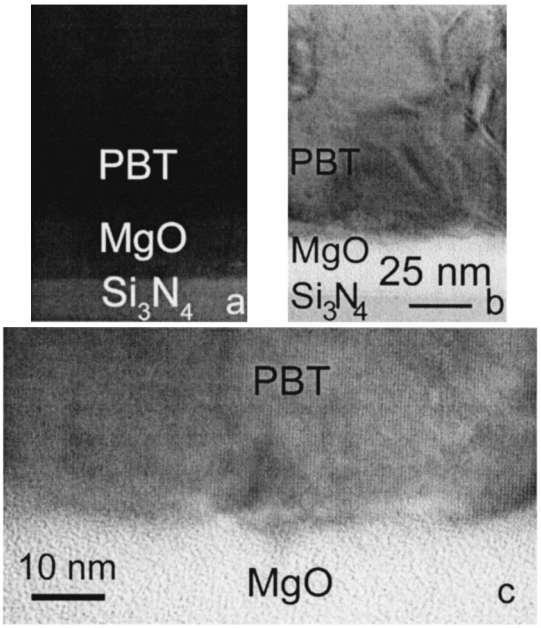

FIG. 5. Cross-section TEM image of MOCVD PBT grown on the biaxially textured MgO. In some areas, the MgO layer appears crystalline (a), whereas in other areas it does not appear to be crystalline (b). (c) High-resolution TEM image of the PBT/MgO interface.

One explanation for the apparently amorphous MgO regions is that these regions were amorphized by the ion milling when they became extremely thin. One TEM image shows a hole in the amorphous-looking MgO, demonstrating the films' thinness.

The diffraction patterns from the plan view and cross-section TEM of the MOCVD PBT on the biaxially textured MgO are included as Figs. 6(a) and 6(b), respectively. In the plan view diffraction pattern [Fig. 6(a)], the arcs of the MgO diffraction spots are somewhat broader than the arcs from the PBT, signifying that the PBT has a narrower in-plane orientation distribution, in agreement with the RHEED measurements, Fig. 4(b). This particular sample was found (by RHEED) to have the MgO template and PBT orientation distributions of 11° and 6° FWHM, respectively. The diffraction pattern also demonstrates that PBT(100) is oriented along the MgO(100). The cross-section TEM diffraction pat-

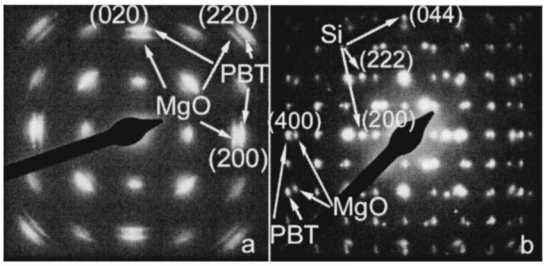

FIG. 6. TEM diffraction patterns of MOCVD PBT on the biaxially textured MgO from (a) the plan view and (b) the cross-section view.

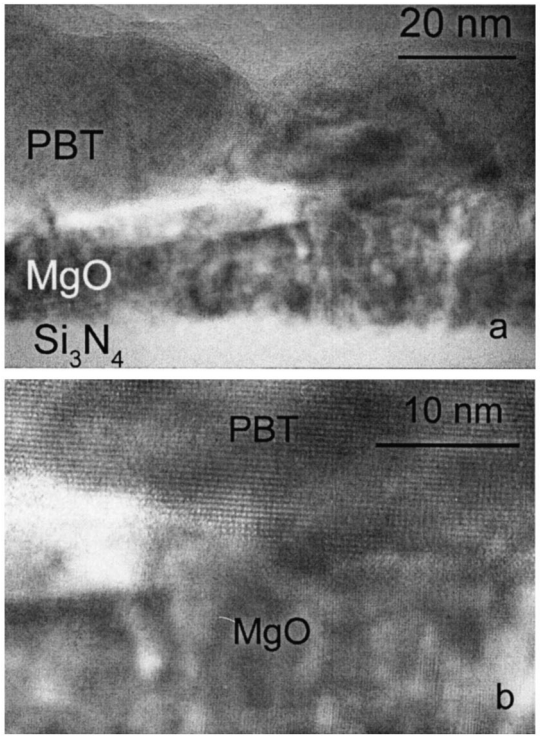

FIG. 7. (a) Cross-section TEM high-resolution image of sol-gel PBT on biaxially textured MgO and (b) closeup of a small interface region from image (a).

tern [Fig. 6(b)] shows a superposition of the diffractions from the Si(100) substrate, the biaxially textured MgO template layer, and the biaxially textured PBT. What is striking about this diffraction pattern is that it illustrates the very narrow out-of-plane orientation distribution achieved through ion-beam-assisted deposition and PBT heteroepitaxy. It also confirms that the PBT(001) and MgO(001) crystal directions are aligned.

The cross-section TEM sample preparation for the sol-gel PBT on the biaxially textured MgO was much more difficult than for the MBE or MOCVD biaxially textured films. Several times during the ion milling, the samples delaminated at the MgO/Si_3N_4 interface before they were thin enough for the cross-section TEM analysis. The failure of the MgO film indicates that it was less robust than the biaxially textured MgO under the MOCVD film and under the MBE film, which were robust during sample preparation. Despite the difficulties in preparing the TEM sample, one area was found that was suitable for TEM imaging.

Figure 7(a) is a high-resolution cross-section TEM image of the sol-gel PBT/MgO biaxially textured interface. The measured PBT thickness is 47 nm and the MgO is 21-nm thick (where there is no thick interface phase). The PBT grain sizes are on the order of 20–30 nm, which is essentially the same size as the 20–25-nm grain sizes observed in the other biaxially textured MgO layers. Some sections of the PBT/MgO interface appear sharp and others appear rough and broad. In the regions of the sample containing a diffuse interface, the MgO layer appears thinner than in those regions containing a sharp interface. Figure 7(b) is a closeup of a transition between a sharp and a broad interface region.

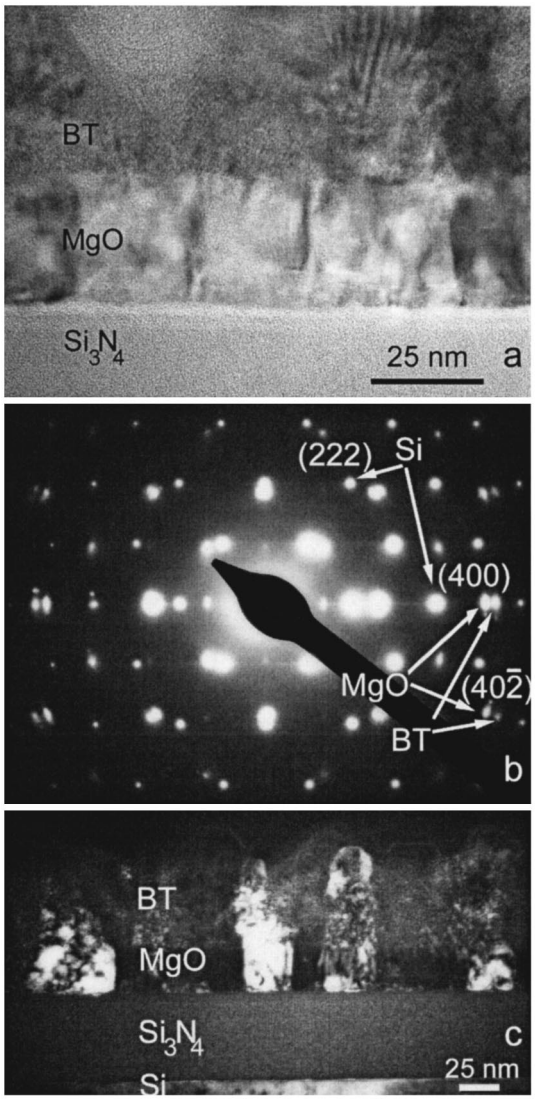

FIG. 8. (a) High-resolution cross-section TEM image of BT on the biaxially textured MgO. (b) Diffraction pattern from the TEM cross-section image (a). The diffraction pattern is a superposition of the diffraction spots from MgO, perovskite BT, and Si. (c) Dark field TEM image of the BT/biaxially textured MgO/amorphous Si_3N_4/Si film stack. MgO grain orientation propagates into the BT layer.

On the right, the MgO and PBT lattice planes are visible and the sharp interface on this small scale appears rough. To the left in Fig. 7(b), the interface opens up with the addition of what appears to be amorphous material between the crystalline MgO and the PBT. Other biaxially textured MgO growth experiments result in the uniformly thick MgO layers [see Fig. 8(a)], so the apparently amorphous material should be part of the biaxially textured MgO layer. These images are not conclusive evidence that the amorphous material is present at the MgO/PBT interface; however, they do demonstrate the inhomogeneity of the interface. The presence of the sharp interfaces between the MgO and the PBT strongly suggests that the amorphous-looking regions are present in the as-grown film and are not a TEM preparation artifact.

The biaxially textured MgO layer in the MBE heterostructure appears very flat and crystalline everywhere. Figure 8(a) is a high-resolution TEM image of the

BT/MgO/Si_3N_4/Si film stack. The high defect density IBAD layer is distinguishable from the homoepitaxial layer and the lattice planes are distinguishable throughout the entire MgO layer, demonstrating that the MgO can survive the TEM sample preparation without becoming amorphous.

A diffraction pattern taken from the film stack is included as Fig. 8(b). The diffraction pattern is a superposition of the diffractions from the silicon substrate, the BT layer, and the biaxially textured MgO. The biaxially textured MgO and BT diffraction spots are small arcs, characteristic of contributions from many grains slightly rotated with respect to each other but narrowly aligned around a common nominal (001) out-of-plane orientation. This diffraction pattern compares very closely to the biaxially textured MOCVD PBT diffraction pattern [Fig. 6(b)]. The main difference between these two patterns is that the weak perovskite diffraction spots are even weaker in the biaxially textured BT diffraction pattern. Furthermore, the absence of extraneous diffraction peaks, which could be associated with Ti-rich phases, supports the conclusion that the $Ba_{0.7}Ti_{1.3}O_3$ is a single phase perovskite.

In the dark field TEM [Fig. 8(c)], the high fidelity of the biaxial texture adoption by the MBE BT film from the MgO template is apparent. The grains defined in the MgO layer propagate directly across the PBT/MgO interface, creating similar oriented grains in the BT film. The RHEED measurements confirm the close relationship between the biaxial texture of the MgO template and the heteroepitaxial BT. Compared to the biaxial texture of its MgO template, the MBE BT out-of-plane orientation distribution is only 0.5° FWHM narrower and the in-plane orientation distribution is only 1.5° FWHM narrower. For the MOCVD and the sol-gel deposition, a change between the biaxial texture of the MgO template and the heteroepitaxial PBT was commonly over 3° FWHM for the out-of-plane orientation distribution and 8° FWHM for the in-plane orientation distribution.

D. Effect of *ex situ* deposition on the MgO template

The TEM, x-ray diffraction, and RHEED measurements create a coherent picture for the biaxial texture inheritance of perovskite ferroelectrics on the biaxially textured MgO. The TEM images show that IBAD MgO has a very high defect density which is reduced but not eliminated in the homoepitaxial layer. We speculate that neither the sol gel nor the MOCVD growth on IBAD MgO layers yields biaxially textured ferroelectric films because the defective IBAD layer is susceptible to damage by the moisture in the atmosphere at the crystal defects. However, the homoepitaxial MgO makes the biaxially textured MgO layer more stable in the atmosphere, resulting in heteroepitaxy of the biaxially textured PBT.

Of the three deposition methods, the sol-gel method most aggressively attacks the biaxially textured MgO layer and at the same time results in the most dramatic in-plane texture improvement. The sol-gel solution contains water, which is known to dissolve and pit the defective MgO films.[20] Additionally, the solution contains acetylacetone. We have observed that acetone vapors effectively degrade the IBAD MgO films and a similar affect might be expected for acetylacetone. We further suggest that the TEM sample preparation was difficult for the biaxially textured sol-gel sample because the MgO layer was degraded during the sol-gel deposition. The high-resolution cross section TEM shows the fully crystalline MgO layers adjacent to the areas with amorphous-looking material at the sol-gel PBT/MgO interface. The data suggest that MgO lattice defects created during IBAD are an important factor in the narrowing of the in-plane orientation distribution of the sol-gel PBT with relation to its biaxially textured MgO template. The IBAD MgO biaxial texturing process produces the fewest number of defects in the most highly in-plane aligned grains. These grains are most likely to survive the sol-gel deposition and provide nucleation sites for the biaxially textured PBT, resulting in a film with a more well-aligned biaxial texture.

As for the sol-gel PBT heteroepitaxy on the biaxially textured MgO, the MOCVD PBT in-plane orientation distribution improved over the in-plane orientation distribution of the MgO template. Because the MOCVD was performed in a separate chamber from the MgO growth, there was an opportunity for the moisture in the atmosphere to degrade the most defective MgO regions enough to reduce the nucleation probability on the heavily damaged, highly in-plane misaligned grains. With minimal atmosphere exposure and without solution to carry away dissolved MgO, the interface between the MOCVD and the biaxially textured MgO remained sharp. The MOCVD film could be crystalline everywhere because the large grain size would enable the crystals to nucleate on the well-aligned grains and overgrow several MgO grains.

Finally, the MBE BT deposition most closely reproduced the biaxial texture of the biaxially textured MgO template. Because the MBE growth was performed *in situ*, the MgO template was preserved as grown and the MBE BT faithfully adopted the texture and grain size from the substrate. The RHEED image from this film was the sharpest of the three ferroelectric films, despite the surface roughness and the nonstoichiometric growth.

The biaxial texture change for the heteroepitaxial films deposited *ex situ* suggests methods for preserving or changing the biaxial texture of the MgO template layer. To protect the template layer against possible atmospheric moisture degradation, the MgO could be coated with other films which are more stable, yet are suitable heteroepitaxial templates for perovskite ferroelectrics. Alternatively, it appears that water selectively attacks the misaligned, more ion-damaged grains, resulting in a template that produces films with an improved biaxial texture by encouraging nucleation on the well-aligned MgO grains. A strategy could be developed for controlled water exposure of the MgO template surface to degrade the unwanted, misaligned grains, followed by annealing, additional MgO growth, or direct hetero epitaxy.

E. Ferroelectric characterization

We have used a modified Park Scientific Instruments Autoprobe CP for DC-EFM to measure the polarization hyster-

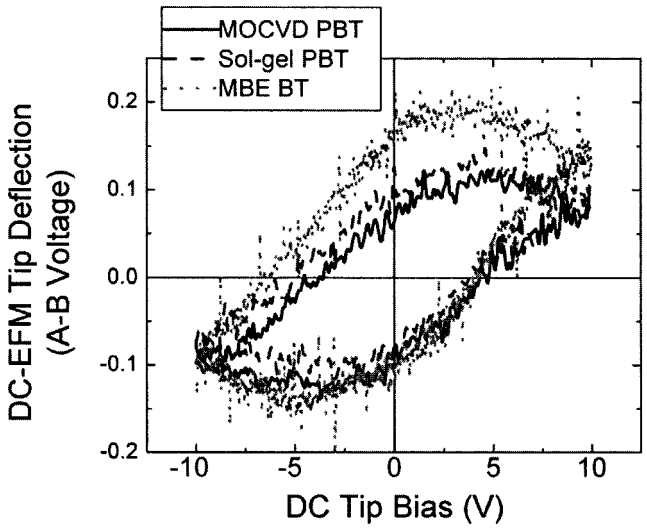

FIG. 9. Polarization hysteresis loops taken with the DC-EFM system biaxially textured sol-gel and MOCVD PBT films, as well as the biaxially textured MBE BT film. Local film polarization is related to the measured DC-EFM tip deflection, measured as the A-B split photodiode voltage.

esis in the biaxially textured PBT and BT films.[14] A local polarization hysteresis loop was acquired by sweeping the substrate bias from 0 to +10 V, down to −10 V, and finally up to 0 V while applying a 3.2 kHz, 5-V ac signal to the AFM tip, and recording the induced tip deflection through a lock-in amplifier as a function of the dc voltage. The hysteresis loop frequency was 5 Hz. Figure 9 shows the polarization hysteresis loops for the biaxially textured PBT, grown using sol gel and MOCVD, as well as for the biaxially textured BT grown using MBE. The polarization hysteresis loop plots the applied dc voltage versus DC-EFM tip deflection (measured as the A-B voltage in the split diode photo detector) because the electric field in the ferroelectric films was unknown and the relationship between the DC-EFM tip deflection and the local film polarization ($\mu C/cm^2$) has not been calibrated. The polarization hysteresis loops demonstrate that the biaxially textured PBT and BT films are ferroelectric and contain 180° switchable domains. By taking local hysteresis loops at several points on the films, we were able to determine that the films are ferroelectric at all points on the size scale of the DC-EFM tip.

IV. CONCLUSIONS

The growth of biaxially textured ferroelectric films, with excellent in-plane and out-of-plane orientation distributions, on MgO templates has been demonstrated. Because the template can be deposited onto amorphous substrates, this represents a significant step toward integrating ferroelectric actuators with Si-based electronics and investigations of the ferroelectric properties of the biaxially textured thin films. The biaxial texture of the MgO template is adopted and even improved by the heteroepitaxial ferroelectric deposition process. The cross-section TEM and RHEED biaxial texture measurements suggest that the *ex situ* (sol gel and MOCVD) heteroepitaxial processes create more highly in-plane aligned ferroelectrics than the MgO template by selectively nucleating on the MgO grains that are well aligned because the defective misaligned grains are degraded by atmospheric moisture. All the PBT and BT ferroelectric films possessed ferroelectric properties and switchable dipole moments, as demonstrated through the DC-EFM polarization hysteresis loops.

ACKNOWLEDGMENTS

The authors would like to thank D. G. Schlom for the helpful discussions about MBE and Carol Garland for the TEM assistance. One of the authors (Y.-B.P.) would like to acknowledge the support of the Postdoctoral Fellowship Program from Korea Science and Engineering Foundation (KOSEF). This work was supported by ARO MURI Grant No. DAAD19-01-1-0517. An additional support has been provided by the National Science Foundation, through the Caltech Center for the Science and Engineering of Materials.

[1] C. P. Wang, K. B. Do, M. R. Beasley, T. H. Geballe, and R. H. Hammond, Appl. Phys. Lett. **71**, 2955 (1997).
[2] Y. Yoneda, T. Okabe, K. Sakaue, and H. Terauchi, Surf. Sci. **410**, 62 (1998).
[3] S. Kim and S. Baik, Thin Solid Films **266**, 205 (1995).
[4] F. Xu, S. Trolier-McKinstry, W. Ren, B. M. Xu, Z. L. Xie, and K. J. Hemker, J. Appl. Phys. **89**, 1336 (2001).
[5] X. D. Wu *et al.*, Appl. Phys. Lett. **67**, 2397 (1995).
[6] G. Burns, Phys. Rev. B **10**, 1951 (1974).
[7] R. T. Brewer, J. R. Groves, P. N. Arendt, and H. A. Atwater, J. Appl. Phys. **93**, 205 (2003).
[8] W. D. Yang, S. C. Pillai, S. W. Boland, and S. M. Haile, Mater. Res. Soc. Symp. Proc. **748**, 165 (2003).
[9] W. J. Desisto and B. J. Rappoli, J. Cryst. Growth **191**, 290 (1998).
[10] C. D. Theis and D. G. Schlom, J. Vac. Sci. Technol. A **14**, 2677 (1996).
[11] J.-P. Locquet and E. Machler, J. Vac. Sci. Technol. A **10**, 3100 (1992).
[12] C. D. Theis and D. G. Schlom, J. Cryst. Growth **174**, 473 (1997).
[13] J. W. Hartman, R. T. Brewer, and H. A. Atwater, J. Appl. Phys. **92**, 5133 (2002).
[14] J. W. Hong, S. I. Park, and Z. G. Khim, Rev. Sci. Instrum. **70**, 1753 (1999).
[15] W. K. Choi, S. K. Choi, and H. M. Lee, J. Mater. Res. **14**, 4677 (1999).
[16] V. Srikant, E. J. Tarsa, D. R. Clarke, and J. S. Speck, J. Appl. Phys. **77**, 1517 (1995).
[17] In *Properties of Crystalline Silicon*, edited by Robert Hull (INSPEC, London, 1999).
[18] K. S. Lee, J. H. Choi, J. Y. Lee, and S. Baik, J. Appl. Phys. **90**, 4095 (2001).
[19] B. Jaffe, W. R. Cook, Jr., and H. Jaffe, *Piezoelectric Ceramics* (Academic, London, 1971), pp. 56–59.
[20] J. A. Mejias, A. J. Berry, K. Refson, and D. G. Fraser, Chem. Phys. Lett. **314**, 558 (1999).
[21] J. R. Groves *et al.*, J. Mater. Res. **16**, 2175 (2001).